Long coherence lifetime and electromagnetically induced transparency in a highly-spin-concentrated solid

Ph. Goldner,* O. Guillot-Noël, F. Beaudoux, Y. Le Du, and J. Lejay
Laboratoire de Chimie de la Matière Condensée de Paris, CNRS-UMR7574, ENSCP, 11 rue Pierre et Marie Curie, 75005 Paris, France

T. Chanelière and J.-L. Le Gouët
Laboratoire Aimé Cotton, CNRS-UPR 3321, Université Paris-Sud, Bâtiment 505, 91405 Orsay Cedex, France

L. Rippe, A. Amari, A. Walther, and S. Kröll
Department of Physics, Lund Institute of Technology, P.O. Box 118, S22100 Lund, Sweden
(Received 12 May 2008; published 9 March 2009)

We have studied a rare-earth-doped crystal, $Pr^{3+}:La_2(WO_4)_3$, which exhibits a high magnetic-moment density. Although the latter favors rare-earth dephasing, a nuclear-spin coherence lifetime of 250 μs has been observed, as well as electromagnetically induced transparency (EIT). This suggests that a broad range of materials could be considered for quantum information applications such as quantum memories for light, where solids are especially attractive. Absorption and dispersion curves are independently in very good agreement with EIT theory. Fano-like profiles have also been observed.

DOI: 10.1103/PhysRevA.79.033809 PACS number(s): 42.50.Gy, 42.50.Md, 71.55.Ht

Coherent light-matter interactions are of particular interest for quantum information processing. Besides applications such as optically controlled qubits or quantum networks, quantum memories for light (QMLs) are actively investigated. Such devices should faithfully store and retrieve photonic quantum states by mapping them onto coherent atomic states. QMLs could have important applications as key elements in quantum repeaters for long-distance quantum cryptography [1–3]. QMLs have been demonstrated in vapors [4,5] but the storage time is limited by atomic movement to a few ms. Applications do however demand much longer storage time, making a solid-state-based QML solution very attractive. Indeed, it was recently demonstrated that a classical pulse could be stored in a nuclear-spin transition for more than 1 s in a rare-earth-doped crystal, $Pr^{3+}:Y_2SiO_5$ [6]. Up to now, this is the only host material in which storage protocols have been studied [7,8]. $Pr^{3+}:Y_2SiO_5$ has very narrow homogeneous linewidths, which originate from the low density of magnetic moments, whose fluctuations cause rare-earth dephasing. However, this crystal intrinsically suffers from a large inhomogeneous broadening due to the difference in ionic radius between Y^{3+} and Pr^{3+} [9,10]. This prevents large optical depths to be reached and thereby limits the QML efficiency. A search for alternative materials is therefore strongly needed. In this paper, we show that it is not necessary to restrict investigations to the very few hosts having similar low magnetic-moment densities. Indeed, long spin coherence lifetime and electromagnetically induced transparency (EIT), on which one of the QML storage protocols is based, have been observed in a rare-earth-doped crystal in which the magnetic-moment density is 7.5 times higher than in Y_2SiO_5. Our observations are perfectly described by the EIT theory when the Rabi frequency and the single-photon detuning of the coupling beam are varied.

*Corresponding author. philippe-goldner@enscp.fr

For these experiments, we used a praseodymium-doped lanthanum tungstate crystal: $La_2(WO_4)_3$. The total magnetic-moment density in this material is $2.2\times10^{22}\mu_B$ cm^{-3}, where μ_B is the nuclear Bohr magneton, whereas it is only $2.9\times10^{21}\mu_B$ cm^{-3} in Y_2SiO_5. This is due to the high nuclear moment ($2.78\mu_B$) of ^{137}La. This crystal was chosen because of the close ionic radii between Pr^{3+} and La^{3+}: $r_{La^{3+}}=1.18$ Å and $r_{Pr^{3+}}=1.14$ Å, as compared to that of $r_{Y^{3+}}$, which is 1.02 Å [11]. This results in an inhomogeneous broadening of Pr^{3+} optical transition that is 15 times smaller than in Y_2SiO_5 at high Pr^{3+} concentration [12]. All experiments were performed on a 0.2% doped Pr^{3+}, 5-mm-thick sample, maintained at 2 K.

EIT is a quantum interference process in which the absorption of the probe vanishes because a strong field couples the excited state to an auxiliary empty state [13,14]. Excitation was provided by a Coherent 699-21 dye laser with a 1 MHz linewidth. Frequency shifts were obtained using a 200 MHz acousto-optic modulator (AOM) mounted in a double-pass configuration. It was followed by a second 360 MHz AOM in which two-color beams could be generated. By strongly focusing into this AOM, the angular separation of the two beams was smaller than the diffraction angle of the focused beam. They were then launched into a single-mode, polarization-maintaining fiber to maximize beam overlap. The maximum power available at the sample entrance side was around 100 mW with a 100-μm spot diameter [15]. When using two-color beams, this experimental setup allowed us to record a beat note for intensity ratios up to 41 dB, the weaker beam having an intensity of about 8 μW. The laser wavelength was set at 602.74 nm (vacuum) in resonance with Pr^{3+} $^3H_4\rightarrow{}^1D_2$ transition. The optical density of the sample was 1.09.

Nuclear-spin coherence lifetimes were measured using two-color optical excitations [16] tuned to the $\pm3/2g\rightarrow\pm5/2e$ and $\pm1/2g\rightarrow\pm5/2e$ transitions (Fig. 1). Two 1-μs-long pulses, separated by a variable delay τ, were

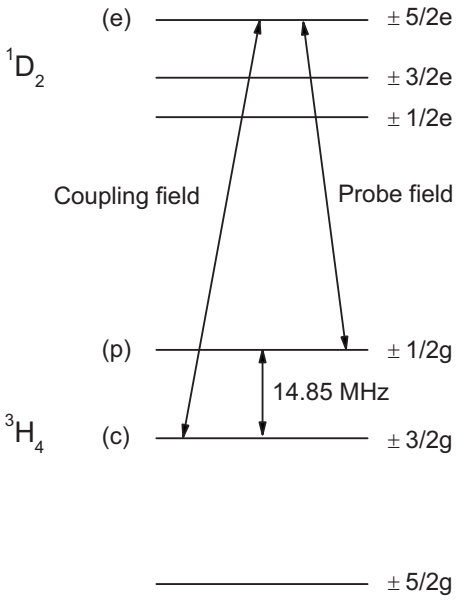

FIG. 1. Hyperfine structure of Pr^{3+} $^3H_4$ and $^1D_2$ levels in $La_2(WO_4)_3$. e, p, and c denote the levels involved in EIT experiments.

shined onto the sample. Nuclear-spin echoes were optically detected by sending a 4-μs pulse along the $\pm 1/2g \rightarrow \pm 3/2e$ and recording the beat note amplitude at the $\pm 3/2g \rightarrow \pm 1/2g$ frequency (14.85 MHz). The coherence lifetime $T_{2\text{spin}}$ of the $\pm 3/2g \rightarrow \pm 1/2g$ transition was deduced from the decrease in the spin-echo amplitude as $\exp(-2\tau/T_{2\text{spin}})$. We found $T_{2\text{spin}}=250\pm 15$ μs, corresponding to a homogeneous linewidth of 1.25 ± 0.1 kHz. Techniques using magnetic fields and radio-frequency pulses which allow an increase in hyperfine coherence lifetimes from 550 μs to 30 s have been demonstrated in $Pr^{3+}:Y_2SiO_5$ [17,18] and should be transposable to our system. Combined with our observation, this suggests that a broad range of materials could be used for QML with long storage times. To further investigate the potential of this material as a QML, we then turned to EIT experiments.

The transitions used for EIT are shown in Fig. 1 and form a three-level Λ system. Because of the inhomogeneous broadening of the $^3H_4 \rightarrow {}^1D_2$ transition, we used optical pumping to select a subensemble of Pr^{3+} ions with an empty $\pm 3/2g$ level and a reduced optical inhomogeneous linewidth of ≈ 1 MHz. The transmission spectrum obtained after this selection is shown in Fig. 2. One can clearly see the $\pm 1/2g \rightarrow \pm 5/2e$ line and the nearly zero absorption at the $\pm 3/2g \rightarrow \pm 5/2e$ position. The two transitions are centered in a wide hole in order to isolate them from the large number of ions absorbing at lower or higher frequencies. This complex selection procedure was carried out using various chirped pulses to empty a spectral region and then pump back a narrow ion ensemble [19]. However, the selection was not entirely successful because of transition coincidences between ions with different energy schemes, and two extra lines denoted by stars appear on the spectrum of Fig. 2.

EIT experiments were then performed by tuning the probe and coupling fields, respectively, to the $\pm 1/2g \rightarrow \pm 5/2e$ and $\pm 3/2g \rightarrow \pm 5/2e$ transitions. The coupling field was first turned on 20 μs before the probe field. Both fields were then turned off simultaneously after 20 μs. To avoid any effect of population pumping by the probe field, the latter was kept at low intensity corresponding to a Rabi frequency of a few kHz. Spectra were taken before and after the probe pulse to check this. Each experimental point in Figs. 3–5 corresponded to 160 averages of a sequence beginning with the selection procedure and followed by the EIT pulses. The averaged signals were then filtered around the beat note frequency with a 1 MHz bandwidth before averaging again the resulting amplitudes and phases over 5 μs.

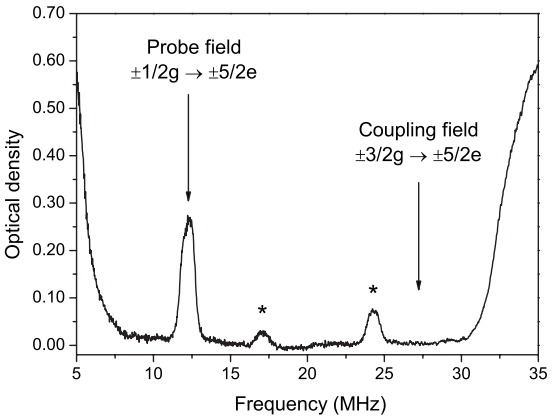

FIG. 2. Spectrum obtained after the selection step prior to EIT experiments. The frequency origin is set at the $\pm 1/2g \rightarrow \pm 1/2e$ transition. Arrows: unwanted ions; see text.

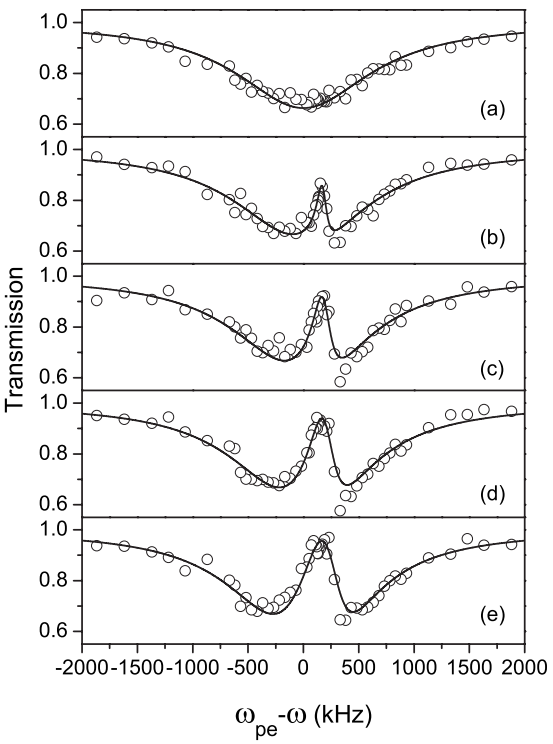

FIG. 3. Transmission of the probe ($\pm 1/2g \rightarrow \pm 5/2e$ transition) as a function of the coupling field Rabi frequency. (a) $\Omega_{ce}=30$, (b) 150, (c) 230, (d) 280, and (e) 340 kHz. Open circles, experimental points; solid line, fitted model.

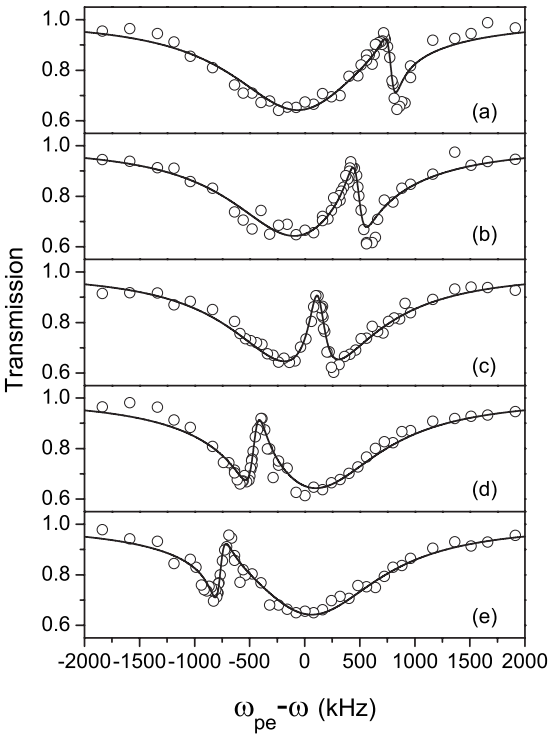

FIG. 4. Transmission of the probe ($\pm 1/2g \rightarrow \pm 5/2e$ transition) as a function of the detuning of the coupling field with respect to the $\pm 3/2g \rightarrow \pm 5/2e$ transition. (a) $\Delta_{ce}=750$, (b) 450, (c) 115, (d) −420, and (e) −735 kHz. Open circles, experimental points; solid line, fitted model.

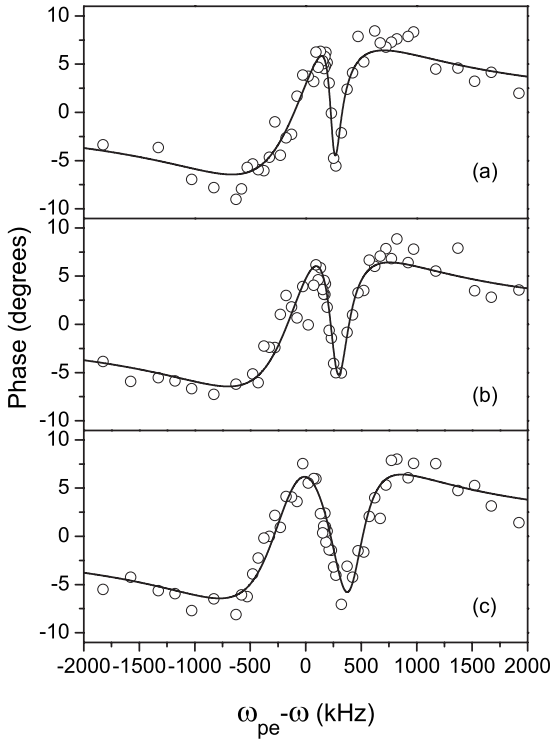

FIG. 5. Phase variation across the $\pm 1/2g \rightarrow \pm 5/2e$ transition as a function of the coupling field Rabi frequency. (a) $\Omega_{ce}=150$, (b) 230, and (c) 340 kHz. Open circles, experimental points; solid line, fitted model.

Figure 3 shows the transmission profile of the $\pm 1/2g \rightarrow \pm 5/2e$ transition as a function of the coupling field Rabi frequency Ω_{ce}. The latter was not precisely known experimentally, and the values quoted in the following were obtained from a fitting procedure described below. At $\Omega_{ce}=30$ kHz, the absorption profile of the $\pm 1/2g \rightarrow \pm 5/2e$ transition has a minimum transmission of 68%. As Ω_{ce} is increased, a transparency window appears with a minimum full width at half maximum (FWHM) of about 70 kHz, limited by the Fourier width of the probe (≈50 kHz). This value gives an upper limit on $\pm 3/2g \rightarrow \pm 1/2g$ linewidth (see below). The transparency window width is much lower than the laser linewidth, which indicates that the effect observed is due to an EIT process. At the center of the transparency window, the transmission reaches 96% at $\Omega_{ce}=350$ kHz, the maximum Rabi frequency we could obtain. In this case, the transparency window had a FWHM of 270 kHz. These results are comparable with those obtained in $Pr^{3+}:Y_2SiO_5$ [6,20,21] and represent a dramatic improvement over previous attempts to see EIT in spin-concentrated hosts such as $Pr^{3+}:LaF_3$, where a 1-MHz-wide window and 5–10 % transparency were observed [22].

Since our three-level system was prepared in a well-defined state, we modeled the transmission profiles to retrieve the characteristic parameters of the system. Under the assumption that (i) the population in state p is close to unity, (ii) population relaxation between levels p and c is negligible, and (iii) the coupling field Rabi frequency Ω_{ce} is constant, the probe transition contribution to the electric susceptibility reads as

$$\chi(\omega) = i\frac{\lambda\alpha_0}{2\pi}\frac{\Gamma_{pe}[\Gamma_{cp}+i(\omega_{pe}-\omega-\Delta_{ce})]}{[\Gamma_{pe}+i(\omega_{pe}-\omega)][\Gamma_{cp}+i(\omega_{pe}-\omega-\Delta_{ce})]+\Omega_{ce}^2}, \tag{1}$$

where α_0, λ, and Γ_{ij}, respectively, stand for the absorption coefficient at line center, the probe transition wavelength, and the half-width at half maximum of the ij transition. The probe transition frequency and the coupling field detuning are, respectively, denoted by ω_{pe} and Δ_{ce}. The low coupling field transmission [Fig. 3(a)] showed that the optical inhomogeneous broadening was described by a Lorentzian profile which was also assumed for the hyperfine transition. This assumption is confirmed by the agreement found between experimental and calculated profiles (see below). Γ_{ij} includes both homogeneous and inhomogeneous contributions. Condition (i) is fulfilled by the selection step described above, whereas levels c and p's lifetime (16 s [12]) verifies assumption (ii). Condition (iii) is discussed below. Transmission was computed from Eq. (1) using the relation

$$T(\omega) = \exp\left(-\frac{2\pi L}{\lambda}\mathrm{Im}[\chi(\omega)]\right), \tag{2}$$

where L is the length of the sample. We then fitted to Eq. (2) seven transmission curves corresponding to Ω_{ce} frequencies evenly spaced between 30 and 350 kHz. During optimization, α_0, Γ_{pe}, Γ_{cp}, and Δ_{ce} values were adjusted simultaneously to all curves, while Ω_{ce} parameters were adjusted independently for each curve. Agreement between theory

and experiments is very good as can be seen in Fig. 3. The adjusted parameters and associated 90% confidence intervals were $\alpha_0=0.82(0.76,0.90)$, $\Gamma_{pe}=667(577,777)$ kHz, $\Gamma_{cp}=22(9.8,36)$ kHz, and $\Delta_{ce}=171(145,225)$ kHz. Taking into account the oscillator strength, fitted Ω_{ce}^2 values (given in Fig. 3) are in good agreement with experimentally measured intensities.

In order to gain a deeper understanding of the phenomenon and to validate our simple model, we then varied the single-photon detuning Δ_{ce} and the coupling field was detuned from the $\pm 3/2g \rightarrow \pm 5/2e$ center frequency (Fig. 4). For detunings larger than ± 300 kHz, an asymmetric profile is observed in contrast with the zero-detuning case. This is due to a quantum interference process between Rayleigh scattering and stimulated Raman scattering similar to a Fano resonance [23]. This is expected under our experimental conditions, and we clearly identified such a profile in a solid. It should be noted that only EIT can produce such an effect as opposed to hole burning. We again fitted the experimental spectra to Eq. (2) with very good agreement (see Fig. 4). Fitted parameters were also consistent with those found in the experiments where Ω_{ce} was varied. It can be noticed, however, that in spectra (a)–(c) in Fig. 4, the low-frequency side of the EIT window is systematically lower in transmission than the calculated one. This could be explained by contribution of ions outside the selected group of ions, such as those located in the left wall of the optically pumped region. This may also explain why this discrepancy is larger when the EIT window is closer to this left wall.

The phase of the probe field is also accessible thanks to our heterodyne detection scheme. It is directly related to the group velocity in the medium and is the basis of slow light experiments. It is simply linked to the susceptibility by

$$\phi(\omega) = \frac{2\pi L}{\lambda}\sqrt{1+\mathrm{Re}[\chi(\omega)]}, \tag{3}$$

and we were also able to model the phase curves obtained for several Ω_{ce} values with parameters consistent with the previous experiments. In particular, the negative slope region, characteristic of slow light, was well reproduced (Fig. 5). The phase dispersion and the absorption profile are connected by causality, irrespective of the physical process at the origin of the transparency window. Therefore, light slowing down can be deduced either from the absorption profile or from phase dispersion and is on the order of ratio between the EIT window width and the absorption coefficient. It is noteworthy that our phase and absorption data consistently lead to a minimum velocity of about 17 km/s, in accordance with theoretical predictions [24] but in strong contrast with some previous experiments [25]. The fundamental causality principle given above suggests that the use of a very weak probe field allowed us to avoid propagation effects which could induce additional delays independently of the EIT transparency window. In our 5-mm-thick sample, the maximum delay experienced by a pulse, with a bandwidth entirely contained inside the EIT window, would be 300 ns. Since we used square pulses with wide bandwidths, we were unable to measure such a short delay. The short delay value also explains that we could accurately model transmission and phase curves although the coupling field was turned off at the same time as the probe field.

In conclusion, a long coherence lifetime and an EIT process with narrow transparency windows and nearly 100% transparency have been observed in a highly-spin-concentrated crystal. In the context of long storage times for quantum memories for light, this result shows that a broad range of materials should be considered, allowing optimization of the physical properties such as optical depth necessary for efficient memories.

The authors would like to acknowledge financial support by the EADS Foundation, the Access to Research Infrastructures activity in the 6th Framework Program of the EU (Contract No. RII3-CT-2003-506350, Laserlab Europe), the European Commission through the integrated project QAP, the Knut and Alice Wallenberg Foundation, and the Swedish Research Council.

[1] J. I. Cirac, P. Zoller, H. J. Kimble, and H. Mabuchi, Phys. Rev. Lett. **78**, 3221 (1997).
[2] H.-J. Briegel, W. Dür, J. I. Cirac, and P. Zoller, Phys. Rev. Lett. **81**, 5932 (1998).
[3] C. Simon, H. de Riedmatten, M. Afzelius, N. Sangouard, H. Zbinden, and N. Gisin, Phys. Rev. Lett. **98**, 190503 (2007).
[4] T. Chanelière, D. Matsukevich, S. Jenkins, S. Lan, T. Kennedy, and A. Kuzmich, Nature (London) **438**, 833 (2005).
[5] M. D. Eisaman, A. André, F. Massou, M. Fleischhauer, A. Zibrov, and M. D. Lukin, Nature (London) **438**, 837 (2005).
[6] J.-J. Longdell, E. Fraval, M.-J. Sellars, and N.-B. Manson, Phys. Rev. Lett. **95**, 063601 (2005).
[7] A.-L. Alexander, J.-J. Longdell, M.-J. Sellars, and N.-B. Manson, Phys. Rev. Lett. **96**, 043602 (2006).
[8] G. Hétet, J. J. Longdell, A. L. Alexander, P. K. Lam, and M. J. Sellars, Phys. Rev. Lett. **100**, 023601 (2008).
[9] K. Holliday, M. Croci, E. Vauthey, and U. P. Wild, Phys. Rev. B **47**, 14741 (1993).
[10] F. Könz, Y. Sun, C. W. Thiel, R. L. Cone, R. W. Equall, R. L. Hutcheson, and R. M. Macfarlane, Phys. Rev. B **68**, 085109 (2003).
[11] R. D. Shannon and G. T. Prewitt, Acta Crystallogr., Sect. B: Struct. Crystallogr. Cryst. Chem. **B25**, 925 (1969).
[12] O. Guillot-Noël, Ph. Goldner, Y. Le Du, P. Loiseau, B. Julsgaard, L. Rippe, and S. Kröll, Phys. Rev. B **75**, 205110 (2007).
[13] S. E. Harris, Phys. Today **50** (7), 36 (1997).
[14] M. Fleischhauer, A. Imamoglu, and J. P. Marangos, Rev. Mod. Phys. **77**, 633 (2005).
[15] L. Rippe, B. Julsgaard, A. Walther, Y. Ying, and S. Kröll, Phys. Rev. A **77**, 022307 (2008).
[16] S. R. Hartmann, IEEE J. Quantum Electron. **4**, 802 (1968).
[17] E. Fraval, M.-J. Sellars, and J.-J. Longdell, Phys. Rev. Lett.

95, 030506 (2005).
[18] E. Fraval, M.-J. Sellars, and J.-J. Longdell, Phys. Rev. Lett. **92**, 077601 (2004).
[19] M. Nilsson, L. Rippe, S. Kroll, R. Klieber, and D. Suter, Phys. Rev. B **70**, 214116 (2004).
[20] K. Ichimura, K. Yamamoto, and N. Gemma, Phys. Rev. A **58**, 4116 (1998).
[21] B. S. Ham, M. S. Shahriar, and P. R. Hemmer, Opt. Lett. **22**, 1138 (1997).
[22] R. Akhmedzhanov, L. Gushin, E. Kuznetsova, A. Litvak, V. Yasenkov, and N. Zharova, J. Mod. Opt. **53**, 2449 (2006).
[23] B. Lounis and C. Cohen-Tannoudji, J. Phys. II **2**, 579 (1992).
[24] E. Kuznetsova, O. Kocharovskaya, P. Hemmer, and M. O. Scully, Phys. Rev. A **66**, 063802 (2002).
[25] A. V. Turukhin, V. S. Sudarshanam, M. S. Shahriar, J. A. Musser, B. S. Ham, and P. R. Hemmer, Phys. Rev. Lett. **88**, 023602 (2001).